Co-combustion Interactions between Teak Sawdust and Sewage Sludge with Additives

Haobin Peng,[a] Yuesheng Li,[b] Guohua Chen,[a,*] and Yunquan Li [b]

The thermal characteristics and kinetics of teak sawdust (TS), sewage sludge (SS), and their blends were evaluated during combustion by thermogravimetric analysis (TGA). The samples were prepared as pure fuel, TS and SS; blends, where TS was mixed with SS at the ratios of 75:25, 50:50, and 25:75; and as fuels with additives, where the fuels above were mixed with activated carbon (AC), CaO, MgO, and ZnO individually at a proportion of 5 wt%. Some characteristic values of combustion were evaluated, such as T_i, T_b, and M_f, and the combustion behaviors of the fuels were compared. The difference between measurement and weighted calculation of the weight left proportion (ΔM), weight loss rate (ΔDTG), and activation energy (ΔE) were introduced for analysis. Blending with teak sawdust improved the combustion performance of sewage sludge. As the content of the sewage sludge increased, the pre-exponential factor varied from 1.76×10^5 s^{-1}(100T) to 1.01×10^1 s^{-1}(100S), while the global activation energy decreased from 74 kJ/mol (100T) to 38 kJ/mol (100S). Sewage sludge burned more completely when blended with teak sawdust at ratios of greater than 50 wt%. All four additives inhibited the oxidation of the blends around the ignition point.

Keywords: Co-combustion; Teak sawdust; Sewage sludge; Synergetic effect; TGA analysis

*Contact information: a: Institute of Safety Science & Engineering, South China University of Technology, 510640, Guangzhou, P. R. China; b: Guangdong Institute of Special Equipment Inspection and Research Shunde Branch, 528300, Foshan, P. R. China; *Corresponding author: mmghchen@scut.edu.cn*

INTRODUCTION

As a byproduct of municipal sewage or industrial wastewater processing, the production of sewage sludge (SS) has increased due to rapid urbanization and industrialization (Fernández-González *et al.* 2017; Fijalkowski *et al.* 2017). Given the presence of harmful substances, such as pathogens, heavy metals, and recalcitrant organic pollutants, a mountainous pile of SS can generate terrible environmental problems in the absence of proper and timely treatment. Certain conventional SS management methods are currently implemented, such as landfilling, composting, and sea filling, all of which are no longer viable or under stringent regulations due to the shortage of land space and environmental concerns (Cieślik and Konieczka 2017; Kacprzak *et al.* 2017). As an effective way to remove the organic pollutants and drastically reduce the volume, incineration/combustion of SS is a promising technology to handle the growing amount of SS. The implementation of these methods also allows the production of some energy during treatment (Syed-Hassan *et al.* 2017).

However, SS incineration/combustion exhibits certain disadvantages, such as high moisture content, high ash content, and low calorific value. Hence, the incineration/ combustion state of isolated SS is difficult to maintain (Kijo-Kleczkowska *et al.* 2015). Blending of some flammable fuels, such as biomass and coal, which has a high volatile

content, low ash content, and high calorific value, with SS has been suggested to improve the SS combustion characteristics (Munir *et al.* 2009). The synergetic co-combustion effect of the SS-biomass blends has been determined by thermogravimetric analysis (TGA) (Xie and Ma 2013; Lin *et al.* 2017). When blended with oil shale, the best promoting effects are observed in the blends with SS at a proportion of 10% (Lin *et al.* 2017). During the co-combustion of paper sludge and rice straw, the smallest average activation energy was observed at a rice straw percentage of 80% in the blends (Xie and Ma 2013). A synergetic effect always occurs between the components during co-combustion. Moreover, the synergetic effect varies at different temperature ranges and in various blend ratios (Peng *et al.* 2015; Deng *et al.* 2016; Roy *et al.* 2018). Thus, to adjust the combustion parameters properly and to efficiently design a combustion system, it is important and practical to investigate the characteristics of synergetic effects between the components throughout the entire co-combustion process.

The co-combustion of biomass and SS will cause pollutant discharge and fouling/slagging. One useful method to reduce pollutant emission and to mitigate fouling/slagging is to blend additives with fuel at a certain proportion. Kaolin, zeolite, dolomite, CaO, and lime are among the frequently used additives (Wang *et al.* 2014; Kafle *et al.* 2017; Roy *et al.* 2018). The addition of kaolin and zeolite 24A reduces the ash-forming tendency of barley straw, when heated at 900 ºC for 1 h, thereby allowing the overall KCl (a low-melting-point substance) to capture the efficiencies of the two additives at values of 60% and 45%, respectively (Kafle *et al.* 2017). The additives $CaCO_3$ and CaO reduce the total emission rate (3.8% to 10.1%) when burnt with raw and carbonized biomass, which is much lower than that of brown coal combustion (33.5% to 37.7%) (Liao *et al.* 2015). With the exception of environmental and ash sintering prevention advantages (Li *et al.* 2016; Qi *et al.* 2017), the additives should also improve combustion properties, such as by shrinking the activation energy of fuel (Roy *et al.* 2018). At present, most reports have focused on the co-combustion of sludge-coal (Lin *et al.* 2017; Zhang *et al.* 2017) or biomass-coal (Gil *et al.* 2010; Kijo-Kleczkowska *et al.* 2016). However, research on the co-combustion behaviors of SS-biomass is relatively scarce. Furthermore, few researchers have investigated the combustion characteristics of SS-biomass mixtures with additives. Consequently, it is necessary to examine the co-combustion behavior and mechanism of additives action in the SS-biomass blends.

In this paper, the combustion characteristics of TS, SS, and their blends were evaluated, and the interaction between the two components was investigated under different ratios. Moreover, the effect of the additives at certain proportions of the TS and SS blends was examined by TGA. The kinetic triplets, which were employed to illustrate the combustion behavior of various processes, were resolved by iso-conversional methods. The results obtained in this work contribute to the characterization of the combustion characteristics of the TS and SS blends and provide references to utilize the fuels.

EXPERIMENTAL

Materials

Sewage sludge (SS) was collected from a sewage treatment plant in Foshan, Guangdong Province, China. Teak sawdust (TS) collected from a furniture factory was taken as the representative material of biomass. The ultimate and proximate analysis results of the two materials are listed in Table 1. The ultimate analysis was determined using a

TruSpec Micro thermal CHNS analyzer (LECO Corporation, Saint Joseph, USA) according to DL/T 568 (2013). The proximate analysis was executed using the methods described in GB/T 28731 (2012).

Table 1. Ultimate and Proximate Analysis of SS and TS

Samples	Ultimate Analysis (wt%, air-dried basis)					Proximate Analysis (wt%, air-dried basis)				LHV * (MJ/kg, air-dried basis)
	C	H	O	N	S	Moisture	Volatile Matter	Fixed carbon	Ash	
SS	19.34	4.08	16.79	3.43	1.24	3.78	40.74	4.14	51.34	9.36
TS	49.96	5.80	37.20	0.01	0.01	4.62	80.29	12.69	2.40	20.04
* LHV, the low heating value as the air-dried basis was determined using an oxygen bomb calorimeter.										

The raw materials of TS and SS were dried at 105 ºC in an oven for 24 h and then pulverized to a size of less than 250 μm in diameter. The TS/SS blends in mass ratios of 25:75, 50:50, and 75:25 were prepared and referred to as 25T75S, 50T50S, and 75T25S, respectively. The activated carbon (AC), calcium oxide (CaO), magnesium oxide (MgO), and zinc oxide (ZnO) were used in the experiments as additives that mixed with the fuel at 5 wt%. All the blends were mixed in a micro rotary mixer for 5 min and then heated at 105 ºC for 2 h to evaporate the moisture prior to its storage in the desiccator. The dry 100% TS and 100% SS were referred to as 100T and 100S, respectively.

Thermogravimetric Analysis

The co-combustion characteristics of SS and TS were tested in an STA-449F5 thermogravimetric analyzer (NETZSCH, Selb, Germany). All the co-combustion experiments were determined at temperatures varying from room temperature to 800 ºC at a heating rate of 20 ºC/min. Each sample was prepared at a weight of approximately 10 mg, and each sample was tested at the same condition in triplicate to minimize the relative error in the TGA data to less than 5 wt%.

Kinetic Analysis

The kinetic parameters associated with solid fuel combustion can be obtained by thermogravimetric analysis. The reactions of the substances are complex processes involving the superposition of several elementary processes, such as nucleation, adsorption, desorption, interfacial reaction, and surface/bulk diffusion. The approach for the computing combustion kinetic rates is based on the Arrhenius equation (Barneto *et al.* 2009; Shen *et al.* 2009; Gil *et al.* 2010). As a result, the separate reactions can be described as follows,

$$\frac{d\alpha}{dt} = kf(\alpha) \quad (1)$$

$$k = A\exp\left[\frac{-E}{RT}\right] \quad (2)$$

where $f(\alpha)$ represents the hypothetical model of the reaction mechanism, k is the reaction rate, A is the pre-exponential factor (min^{-1}), E is the activation energy (kJ/mol), T is the absolute temperature (K), t is the time (min), R is the universal gas constant (8.314

kJ/(mol·K)), and α is the degree of conversion, which is defined as follows,

$$\alpha = \frac{m_0 - m_t}{m_0 - m_f} \quad (3)$$

where m_0 and m_t represent the masses at $t = 0$ and $t = t$, respectively, and m_f is the final mass of the sample.

Table 2. Expressions for the Most Common Reaction Mechanisms in Solid Fuel Reactions

Reaction model	$g(\alpha)$
Reaction order	
O_0	α
O_1	$-\ln(1-\alpha)$
O_2	$-(1-\alpha)^{-1}$
Phase boundary-controlled reaction	
R_2	$1-(1-\alpha)^{1/2}$
R_3	$1-(1-\alpha)^{1/3}$
Power law	
P_1	$\alpha^{1/4}$
P_2	$\alpha^{1/3}$
P_3	$\alpha^{1/2}$
P_4	$\alpha^{3/2}$
Nucleation and growth (Avrami-Erofeev equation)	
N_1	$[-\ln(1-\alpha)]^{1/1.5}$
N_2	$[-\ln(1-\alpha)]^{1/2}$
N_3	$[-\ln(1-\alpha)]^{1/3}$
N_4	$[-\ln(1-\alpha)]^{1/4}$
Diffusion	
D_1	α^2
D_2	$(1-\alpha)\ln(1-\alpha)+\alpha$
D_3	$[1-(1-\alpha)^{1/3}]^2$
D_4	$1-2/3\alpha-(1-\alpha)^{2/3}$

For a constant heating rate (K/min) during combustion, specifically $\beta = dT/dt$, Eq. 1 can be transformed to:

$$\frac{dx}{f(\alpha)} = \frac{k}{\beta dt} \quad (4)$$

Integrating Eq. 4 gives:

$$g(a) = \int_0^{\alpha} \frac{dx}{f(\alpha)} = \frac{A}{\beta}\int_{T_0}^{T} \exp\left[\frac{-E}{RT}\right] dT \quad (5)$$

Equation 5 can be integrated using the Coats-Redfern method (Coats and Redfern 1964), thereby yielding:

$$\ln\left(\frac{g(\alpha)}{T^2}\right) = \ln\left[\frac{AR}{\beta E}\left(1-2\frac{RT}{E}\right)\right] - \frac{E}{RT} \quad (6)$$

Generally, the term $2RT/E$ can be neglected, since it was much lower than 1 (Liu *et al.* 2002). Both the combustion temperatures range and most values of E in the expression $\ln[AR/\beta E(1\text{-}2RT/E)]$ in Eq. 7 are essentially constant (Zhou *et al.* 2006). Thus, if the correct expression of $g(\alpha)$ was used, the plot of $\ln[g(\alpha)/T^2]$ against $1/T$ should give a straight line with a high correlation coefficient from which the values of E and A could be calculated from the slope of the line and the intercept term in Eq. 6, respectively. In this work, the nearest expression to describe the biomass thermal decomposition was determined by substitution and comparison. The functions in $g(\alpha)$, which refer to the different reaction models, are presented in Table 2 (White *et al.* 2011).

Combustion Comprehensive Factor (CCF)

To assess the combustion behaviors of TS and SS, a comprehensive index (CCF) for their combustion characteristics was introduced and calculated as follows (Xie and Ma 2013; Lin *et al.* 2017),

$$\mathrm{CCF} = \frac{(dw/dt)_{\max}(dw/dt)_{\mathrm{mean}}}{T_i^2 T_b} \quad (7)$$

where $(dw/dt)_{\max}$ and $(dw/dt)_{\mathrm{mean}}$ represent the maximum and the average weight loss rate (wt%/min), respectively, and T_i and T_b are the ignition and burnout temperatures (°C), respectively. The CCF comprehensively characterized the burning behavior of the fuel. A larger CCF value represented an easily burned sample.

RESULTS AND DISCUSSION

Combustion Behaviors of SS and TS

Figure 1 presents the TGA-DTG curves of 100T and 100S at a heating rate of 20 °C/min. Generally, biomass combustion includes three stages: moisture evaporation (stage I), devolatilization and volatile combustion (stage II), and fixed-carbon burning (stage III) (Yang *et al.* 2004; Fang *et al.* 2013). In this research, stage I was obscure because all the samples were desiccated in advance. However, the latter two stages were identified by the formation of obvious peaks on the DTG curves. As shown in Fig. 1, stage II presents the devolatilization and volatile combustion as well as the formation of fixed carbon, and stage III exhibits the burning of the fixed carbon (Szemmelveisz *et al.* 2009; Tang *et al.* 2011). The first visible weight-loss peak corresponding to devolatilization and volatile combustion resulted in the formation of fixed carbon, and the succeeding peak involved the process of fixed carbon combustion. As the temperature rose, following the end of homogeneous combustion, a second weight-loss peak was observed on the DTG curve of 100T, whereas this was imperceptible on the DTG curve of 100S. On account of the fixed carbon content of 100T (12.69 wt%), which was much higher than that of 100S (4.14 wt%),

the heterogeneous combustion behavior of 100T was more remarkable than that of 100S at the stage of post-homogeneous combustion, *i.e.*, stage III. As shown in Fig. 1, the temperature corresponding to the highest decomposition rate (the first weight-loss peak on the DTG curve) of 100S was obviously lower than that of 100T. Moreover, the temperature range covering devolatilization and the homogeneous combustion process of 100S was broader than that of 100T, and this thereby indicated that the 100S contained some small molecules with lower thermal decomposition temperatures (Akinrinola *et al.* 2014). It became clear that the homogeneous combustion performance of 100S at lower temperatures was more intensive than that of 100T.

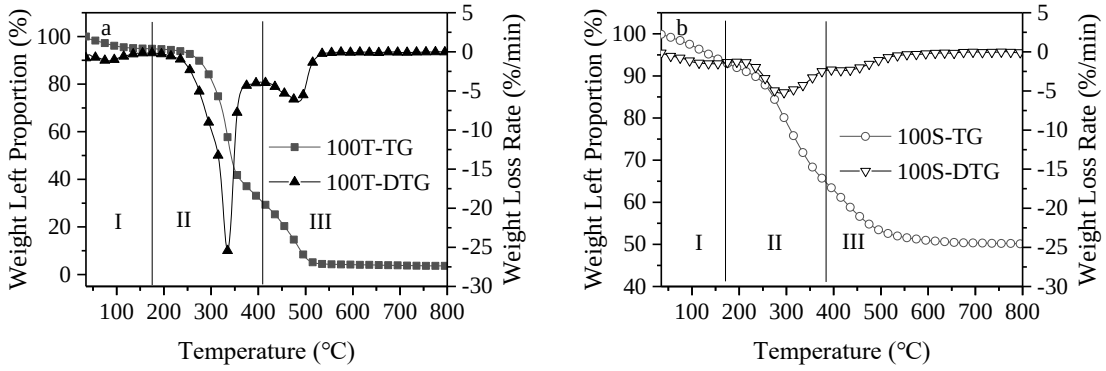

Fig. 1. TGA-DTG curves of 100T and 100S at a heating rate of 20 °C/min: (a) 100T and (b) 100S

Several relevant combustion characteristic parameters, including T_i, T_p, and T_b, are summarized in Table 3. The variable T_i represents the ignition temperature of the sample, which can be determined according to the TGA-DTG curves. The variable T_b is the burnout temperature, determined as the temperature when the weight loss rate reaches 0.1 wt%/min at the end of combustion. The maximum weight loss rate $(dw/dT)_{max}$ and the corresponding temperature (T_p) represent the combustibility and reactivity of the fuels. Many fuels have more than two weight-loss peaks during combustion because their combustible contents burn at different temperature ranges (Chen *et al.* 2017; Kumar and Singh 2017; Huang *et al.* 2018). Generally, the sooner the T_P appears and the greater the $(dw/dT)_{max}$ is, the easier the fuel ignites. On the DTG curve, a vertical line was drawn through point A, which corresponded to the weight-loss peak of devolatilization that intersected the TG curve in point B. In addition, the tangent line through B was drawn to intersect a horizontal line that passed the weight loss beginning point of TGA curve in point C such that the temperature corresponding to C was defined as T_i (Wang *et al.* 2009). As observed in Table 3, the T_i of 100T was 51 ºC higher than that of 100S, representing that there were differences in the structures and ingredients between the two (Chen *et al.* 2017). The 100S mainly contained lower organic substances such as fulvic acids, proteins, and polycyclic aromatic hydrocarbons, which are easier to decompose (Kulikowska 2016; Wang *et al.* 2016; Chen *et al.* 2017), thereby resulting in a stronger ignition performance than 100T. The burnout temperature of 100S was more than 100 ºC higher than that of 100T because the former contained more noncombustible components than the latter. The residue of 100T (3.6 wt%) was much higher than that of 100S (50.1 wt%), which was highly consistent with the ash content in Table 1. As shown in Table 3, the maximum weight loss rate of TS was higher than that of 100S, which was attributed to the quicker and stronger release and burning of the volatiles. The homogeneous combustion performance of 100S in stage II exceeded that

of 100T. However, the heterogeneous combustion performance of 100T in stage III was more remarkable than that of 100S. The combustion behavior index (CCF) of 100T was much higher (32.19×10^{-7}) than that of 100S (2.54×10^{-7}), and thereby indicated that 100T was easier to burn than 100S when the whole combustion process was concerned.

Table 3. Pivotal Points of the TGA-DTG Curves for the Combustion Process of TS and SS

Pivotal Points	TS		SS	
	Stage II	Stage III	Stage II	Stage III
T_{id} * (°C)	177	—	200	—
T_i (°C)	303	—	252	—
T_b (°C)	—	557	—	664
T_{ip} * (°C)	177	405	200	397
T_{fp} * (°C)	405	557	397	663
T_p (°C)	335	483	293	415
$(dw/dT)_{max}$ (wt%/°C)	25.4	6.4	5.3	2.4
M_f * (%)	—	3.6	—	50.1
CCF ($\times 10^{-7}$)	32.19		2.54	
* T_{id} - initial decomposition temperature; T_{ip} - initial peak temperature; T_{fp} - final peak temperature; and M_f - residue left				

The Interaction between TS and SS during Co-combustion

To investigate the interaction between 100T and 100S during co-combustion, the differences of the parameters, which symbolized the combustion behavior, were calculated as follows,

$$\Delta W = W_{\exp} - W_{\text{cal}} = W_{\exp} - (W_{\text{TS}} \times TS\% + W_{\text{SS}} \times SS\%) \quad (8)$$

where W_{exp} and W_{cal} are the tested and calculated results of the weight left proportion (M), weightlessness rate (DTG), or activation energy (E) of each sample, respectively; W_{TS} and W_{SS} are the individual weight left proportions, weight-loss rates, or activation energies of 100T and 100S at a certain temperature, respectively; TS% and SS% are the original ratios of 100T and 100S within the blend, respectively; and ΔW refers to the ΔM, ΔDTG, and ΔE.

If the residue left by burning the blend weighed more than what was calculated based on the separately burned components, symbolized as $\Delta M > 0$, then the interaction between the components inhibited the combustion. On the contrary, if $\Delta M < 0$, then the interaction promoted the combustion. A value of $\Delta M < 0$ at the end of the combustion indicated that the interaction reduced the amount of residue, which was beneficial for the burnout characteristic of the blend. If the burning velocity of the blend was faster than what was calculated based on the separately burned components, *i.e.*, $\Delta DTG < 0$, the interaction between the components was promoted. However, if $\Delta DTG > 0$, the interaction obstructed the combustion at the corresponding temperature. The ΔM and ΔDTG curves are illustrated in Fig. 2a and Fig. 2b, respectively.

According to Fig. 2a, most of the ΔM curves for the blends of 25T75S and 50T50S stood above the X-axis and $\Delta M > 0$ at the end of combustion, which illustrated that the interactions between 100T and 100S at the respective ratios scarcely benefited the burnout property of the blends. However, the value of ΔM decreased as the ratio of 100T increased. In the temperature range of 350 ºC to 500 ºC, under which hemicellulose and cellulose decomposed and fixed carbon came into being (Papari and Hawboldt 2015), most of the ΔM curves laid beneath the X-axis, especially for the blends of 75T25S, which indicated

that the interaction among the components of 100T and 100S favored the decomposition of the hemicellulose and cellulose and benefited the fixed carbon combustion behavior of 75T25S. In addition, at the temperature range above 600 ºC, only the Δ*M* curve of 75T25S was beneath the X-axis among the three blends, which illustrated that the beneficial interaction to the burnout feature occurred only when the ratio of 100T was higher than that of 100S. It can be inferred that the catalysis of 100T can improve the ash-forming characteristics of the co-combustion with 100S (Link *et al.* 2018).

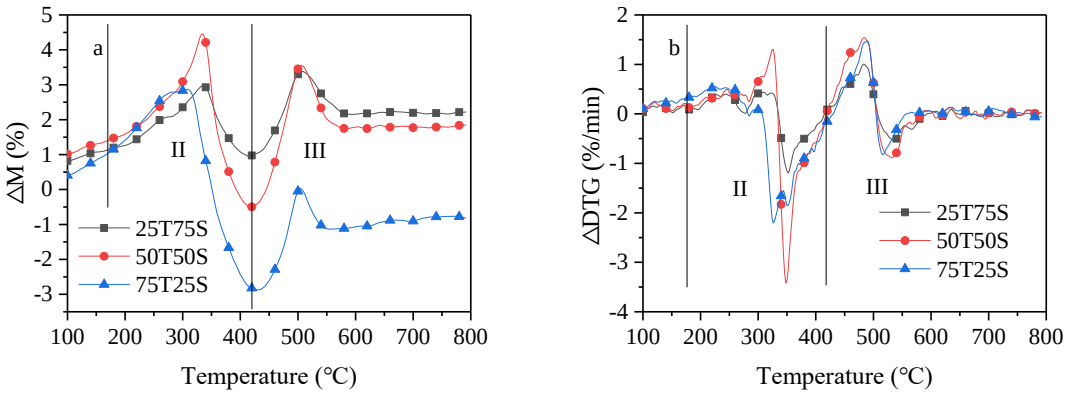

Fig. 2. Variation profiles of Δ*M* and Δ*DTG* at different blending ratios (20 °C/min)

According to Fig. 2b, all of the three blends exhibited Δ*DTG* > 0 at a temperature range of 100 ºC to 280 ºC, which indicated that the interaction between the components inhibited the oxidation. The interaction impeded the devolatilization even if the blends were not ignited (Li *et al.* 2016). At a temperature range of 280 ºC to 580 ºC, the interaction of the main combustion process tended to be intense, given that the value of Δ*DTG* alternated above or below zero. For the samples of 25T75S and 75T25S, the interaction promoted the combustion throughout the temperature range of 280 ºC to 420 ºC, given that Δ*DTG* < 0. In comparison, the interaction in the sample of 50T50S hindered the combustion at the temperature range of 280 ºC to 350 ºC, which covered the ignition point for Δ*DTG* > 0, and thereby promoted combustion at a temperature range of 350 ºC to 420 ºC, given that Δ*DTG* < 0. At a temperature range of 420 ºC to 500 ºC, wherein the combustion developed to the fixed carbon combustion stage (stage III), the interactions for all of the three blends hindered their combustion for Δ*DTG* > 0 conformably. In comparison, at a temperature range of 500 ºC to 600 ºC, specifically the burnout stage, the interactions promoted the oxidation such that Δ*DTG* < 0, which thereby accelerated the burnout process of the samples. Subsequently, at a temperature range above 600 ºC, faint interactions were observed among the residues such that the curve of Δ*DTG* fluctuated surrounding the X-axis slightly. In summary, within a temperature range of 280 ºC to 420 ºC, *i.e.*, stage II, the concluded integration from Δ*DTG* was negative, which meant that the devolatilization and volatile combustion of the blends were promoted (Li *et al.* 2016). At a temperature range of 420 ºC to 500 ºC, *i.e.*, stage III, the combustion was inhibited given that Δ*DTG* > 0 for the blends, namely that the fixed carbon combustion was obstructed (Singh and Zondlo 2017). When the temperature range was above 600 ºC, Δ*DTG* ≈ 0, and thereby resulted in weak interaction because most of the combustible substances had been consumed.

Figure 3 indicates that the shapes of the Δ*E* profiles of the three blends tested were

similar during combustion. At the mid-temperature range, which approximately represented the devolatilization and volatile combustion stage, $\Delta E > 0$, which thereby indicated that the activation energy increased because of the synergetic effect between 100T and 100S. As a result, the combustion was inhibited compared to the low and high temperature zones, *i.e.*, the desiccation, early devolatilization, and fixed carbon oxidation stages, $\Delta E < 0$, which promoted combustion. However, a comparison of the ΔE profile to ΔM and ΔDTG profiles in Fig. 2 indicated that the evolutions of the three indices were not exactly the same, which thereby indicated the presence of some differences between the three mechanisms that characterized the combustion intensity. The isolate activation energy coefficient did not fully characterize the conversion rate, which must be calculated by the activation energy (E) and the pre-exponential factor (A) according to the Arrhenius equation (Wang *et al.* 2018). As a result, the determination of whether the synergistic effects promoted or inhibited the co-combustion process was mainly based on ΔM and ΔDTG.

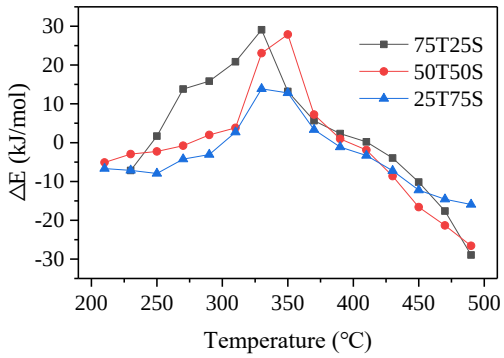

Fig. 3. Variation profiles of ΔE at different blending ratios (20 °C/min)

Effects of the Additives

The TGA-DTG curves of the individual 100T and 100S with additives at a heating rate of 20 ºC/min are illustrated in Fig. 4. The addition of AC resulted in lowering T_3 from 483 ºC to 470 ºC when the 100T was individually burned. In addition, the respective highest weight loss rate increased from 6.4% to 6.7%, which indicated that the addition of AC benefited the fixed carbon combustion of 100T (Gil *et al.* 2015). Moreover, in view of M_f, CaO was the most unfavorable additive to 100T because the value of M_f was 7.9%, more than twice as much as that of 100T to burn alone. As presented in Fig. 4b, a certain difference was observed between the five DTG curves of 100S alone and with various additives. Specifically, the T_2 of the combustion with CaO increased from 253 ºC to 257 ºC, and the respective weight loss rate abated from 5.2% to 4.9%. In addition, a new weight loss peak appeared on the DTG curve of 100S burnt with AC at 562 ºC, which represented the fact that AC could promote the fixed carbon combustion behavior of 100S (Singh and Zondlo 2017), while no noticeable peak above 400 ºC was observed on the DTG curve of 100S burnt alone. Furthermore, new peaks were observed on the DTG curves at the temperatures around 660 ºC within the burnout processes with CaO and MgO, which thereby illustrated that the additives of CaO and MgO also promoted the burnout behavior of 100S by catalyzing the decomposition of inorganic minerals (Kijo-Kleczkowska *et al.* 2016). A comparison of the TGA curves of 100T and 100S with additives indicated that only AC reduced the residue left of 100S, which helped to burn the individual 100S more completely. In view of the 100S, the effect was different when burning in the presence of

various additives. In the case of burning alone or with ZnO, the weight loss proportion of devolatilization and volatile combustion at about 194 ºC and 529 ºC were 37.9% and 40.2%, respectively. As a result, ZnO benefited the combustion performance of 100S at stage II. The individual combustion of 100S with CaO and MgO exhibited a lengthened stage II temperature range from a lower limit of 406 ºC to an upper limit of 590 ºC, which thereby indicated the promotion of the devolatilization and volatiles combustion process.

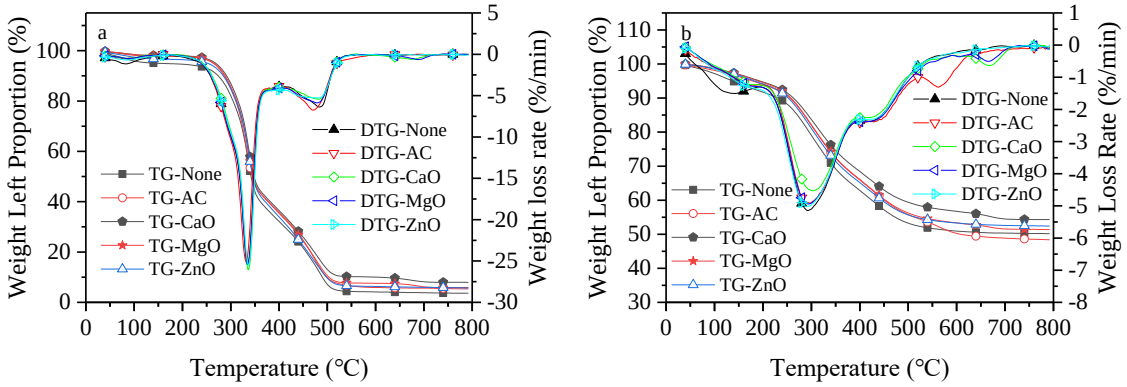

Fig. 4. TGA-DTG curves of 100T and 100S with additives at a heating rate of 20 °C/min: (a) 100T and (b) 100S

Figure 5 presents the Δ*DTG* profile values with the different additives and the effects of the additives to the blends.

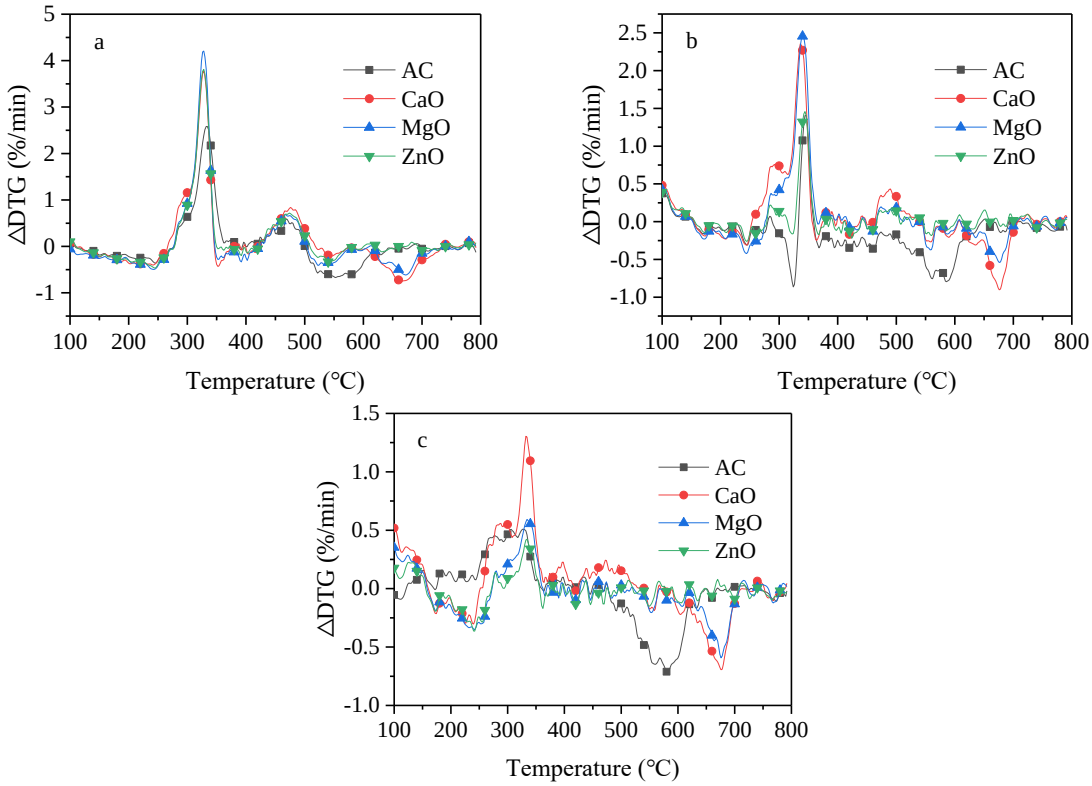

Fig. 5. Variation profiles of the Δ*DTG* curves with additives at a heating rate of 20 °C/min: (a) 75T25S; (b) 50T50S; and (c) 25T75S

Table 4. Activation Energies (*E*, kJ/mol), Pre-exponential Factors (*A*, s^{-1}) and Correlation Coefficients (R^2) Values of the Teak-sludge Blends with Additives at 20 °C/min

Additives	100T			75T25S			50T50S			25T75S			100S		
	E	*A*	R^2	*E*	*A*	R^2	*E*	*A*	R^2	*E*	*A*	R^2	*E*	*A*	R^2
None	74.65	1.76×10^5	0.95	74.75	1.28×10^5	0.92	52.97	1.09×10^3	0.94	43.56	1.27×10^2	0.95	32.19	1.01×10^1	0.97
AC	90.77	3.08×10^6	0.93	71.00	5.26×10^4	0.92	56.30	2.13×10^3	0.95	40.77	6.81×10^1	0.95	37.85	2.68×10^1	0.97
CaO	93.20	4.29×10^6	0.93	70.79	4.83×10^4	0.92	57.39	2.02×10^3	0.95	46.68	1.93×10^2	0.96	38.65	2.63×10^1	0.97
MgO	92.07	3.82×10^6	0.93	74.86	1.01×10^5	0.92	55.49	1.50×10^3	0.95	45.86	1.93×10^2	0.96	39.68	3.86×10^1	0.97
ZnO	83.65	8.46×10^5	0.94	69.89	4.20×10^4	0.92	57.91	2.57×10^3	0.94	44.18	1.46×10^2	0.96	38.41	3.19×10^1	0.97

According to Fig. 5, in the three blends with various blending ratios, the most remarkable positive Δ*DTG* peaks were coincidently formed at about 320 ºC, which thereby illustrated that all the four additives were inhibitive to the blends around the ignition point, *i.e.*, the temperature zone at which devolatilization occurred and volatile combustion began. Furthermore, as the proportion of 100S increased, the values of the positive peaks decreased such that the prohibitive synergetic effect between the additives and the blends was abated. Moreover, the most noticeable negative peaks on three Δ*DTG* curves of AC were observed at about 575 ºC, and those of CaO and MgO were observed at about 680 ºC, which thereby illustrated that the maximum synergistic effects of the blends with the different proportions always occurred in the same temperature region. In contrast, the Δ*DTG* curve of ZnO always fluctuated near the X-axis and the values of peaks were almost at the minimums of the four curves, which thereby indicated that the synergetic effect of ZnO was the weakest of the four additives. The effects of the additives were not remarkable or roughly more promotive prior to ignition and during the fixed carbon combustion stage because the curves were all near or beneath the X-axis at the respective temperature regions. In comparison, according to the Δ*DTG* curve, the interaction during combustion of AC was the least of the four additives, which thereby indicated that the AC might have been the most promotive additive in the entire combustion process of the three blends.

Table 4 presents the comparisons of the global activation energies (E_{glo}) and pre-exponential factors of the five tested samples with or without additives, respectively. For the blends without additives, the values of E_{glo} decreased as the ratios of SS increased, *e.g.*, from 74 kJ/mol (100T) to 32 kJ/mol (100S), which promoted the reactivity of the sample. The values of *A* also exhibited decreased orders of magnitude, *e.g.*, from 1.76×10^5 s^{-1} (100T) to 1.01×10^1 s^{-1} (100S), which inhibited the combustion behavior of the sample, though this exhibited a lower effect than the activation energy in the global kinetics (Papari and Hawboldt 2015). When added with additives, the E_{glo} values of 100T, 50T50S, and 100S increased, and the E_{glo} values of 75T25S decreased, except for 75T25S-MgO. In addition, the E_{glo} values of 25T75S were very close. Moreover, for the same sample with different additives, the *A* value did not vary beyond a certain order of magnitude, *e.g.*, the *A* values of 75T25S with different additives varied from 4.20×10^4 s^{-1} (with ZnO) to 1.01×10^5 s^{-1} (with MgO). As a result, the synergetic effects of the additives to the samples were different and exhibited no obvious regularity, which was mostly a result of either the comprehensively involved chemical mechanisms or physical characteristics (López *et al.* 2014; Shang *et al.* 2015).

CONCLUSIONS

1. The co-combustion characteristics of teak sawdust and sewage sludge with additives were studied at different mixing ratios. The ignition point of sewage sludge (252 °C) was lower than that of teak sawdust (303 °C), while the CCF value of teak sawdust (32.19×10^{-7}) was higher than that of sewage sludge (2.54×10^{-7}).
2. Blending with teak sawdust could improve the combustion performance of sewage sludge. When the content of teak sawdust increased, the pre-exponential factor value increased by orders of magnitude, and the activation energy value rose by the same order of magnitude. Sewage sludge burned more completely when blended with teak sawdust at ratios of greater than 50 wt%.

3. When the blends were burned without additives, devolatilization and volatile combustion were promoted, and the fixed carbon combustion was inhibited. In addition, the burnout velocity was accelerated. All of the four additives inhibited the oxidation of the blends around the ignition point.

ACKNOWLEDGMENTS

This work was supported by the Natural Science Foundation of China (No. 51503067). The authors would like to thank LetPub (www.letpub.com) for providing linguistic assistance during the preparation of this manuscript.

REFERENCES CITED

Akinrinola, F. S., Darvell, L. I., Jones, J. M., Williams, A., and Fuwape, J. A. (2014). "Characterization of selected Nigerian biomass for combustion and pyrolysis applications," *Energ. Fuel* 28(6), 3821-3832. DOI: 10.1021/ef500278e

Barneto, A. G., Carmona, J. A., Alfonso, J. E. M., and Blanco, J. D. (2009). "Kinetic models based in biomass components for the combustion and pyrolysis of sewage sludge and its compost," *J. Anal. Appl. Pyrol.* 86(1), 108-114. DOI: 10.1016/j.jaap.2009.04.011

Chen, J., Liu, J., He, Y., Huang, L., Sun, S., Sun, J., Chang, K., Kuo, J., Huang, S., and Ning, X. (2017). "Investigation of co-combustion characteristics of sewage sludge and coffee grounds mixtures using thermogravimetric analysis coupled to artificial neural networks modeling," *Bioresource Technol.* 225, 234-245. DOI: 10.1016/j.biortech.2016.11.069

Cieślik, B., and Konieczka, P. (2017). "A review of phosphorus recovery methods at various steps of wastewater treatment and sewage sludge management. The concept of "no solid waste generation" and analytical methods," *J. Clean. Prod.* 142, 1728-1740. DOI: 10.1016/j.jclepro.2016.11.116

Coats, A. W., and Redfern, J. P. (1964). "Kinetic parameters from thermogravimetric data," *Nature* 201, 68-69. DOI: 10.1038/201068a0

Deng, S., Wang, X., Tan, H., Mikulčić, H., Yang, F., Li, Z., and Duić, N. (2016). "Thermogravimetric study on the co-combustion characteristics of oily sludge with plant biomass," *Thermochim. Acta* 633, 69-76. DOI: 10.1016/j.tca.2016.03.006

DL/T 568 (1995). "Fast test methods for ultimate analysis of fuel by infrared absorption and thermal conductivity," Standardization Administration of China, Beijing, China.

Fang, X., Jia, L., and Yin, L. (2013). "A weighted average global process model based on two−stage kinetic scheme for biomass combustion," *Biomass Bioenerg.* 48, 43-50. DOI: 10.1016/j.biombioe.2012.11.011

Fernández-González, J. M., Grindlay, A., Serrano-Bernardo, F., Rodríguez-Rojas, M., and Zamorano, M. (2017). "Economic and environmental review of waste-to-energy systems for municipal solid waste management in medium and small municipalities," *Waste Manage.* 67, 360-374. DOI: 10.1016/j.wasman.2017.05.003

Fijalkowski, K., Rorat, A., Grobelak, A., and Kacprzak, M. J. (2017). "The presence of contaminations in sewage sludge – The current situation," *J. Environ. Manage.* 203, 1126-1136. DOI: 10.1016/j.jenvman.2017.05.068

GB/T 28731 (2012). "Proximate analysis of solid biofuels," Standardization Administration of China, Beijing, China.

Gil, M. V., Casal, D., Pevida, C., Pis, J. J., and Rubiera, F. (2010). "Thermal behaviour and kinetics of coal/biomass blends during co-combustion," *Bioresource Technol.* 101(14), 5601-5608. DOI: 10.1016/j.biortech.2010.02.008

Gil, M. V., García, R., Pevida, C., and Rubiera, F. (2015). "Grindability and combustion behavior of coal and torrefied biomass blends," *Bioresource Technol.* 191, 205-212. DOI: 10.1016/j.biortech.2015.04.117

Huang, L., Xie, C., Liu, J., Zhang, X., Chang, K., Kuo, J., Sun, J., Xie, W., Zheng, L., Sun, S., Buyukada, M., and Evrendilek, F. (2018). "Influence of catalysts on co-combustion of sewage sludge and water hyacinth blends as determined by TG-MS analysis," *Bioresource Technol.* 247, 217-225. DOI: 10.1016/j.biortech.2017.09.039

Kacprzak, M., Neczaj, E., Fijałkowski, K., Grobelak, A., Grosser, A., Worwag, M., Rorat, A., Brattebo, H., Almås, Å., and Singh, B. R. (2017). "Sewage sludge disposal strategies for sustainable development," *Environ. Res.* 156, 39-46. DOI: 10.1016/j.envres.2017.03.010

Kafle, S., Euh, S. H., Cho, L., Nam, Y. S., Oh, K. C., Choi, Y. S., Oh, J.-H., and Kim, D. H. (2017). "Tar fouling reduction in wood pellet boiler using additives and study the effects of additives on the characteristics of pellets," *Energy* 129, 79-85. DOI: 10.1016/j.energy.2017.04.105

Kijo-Kleczkowska, A., Środa, K., Kosowska-Golachowska, M., Musiał, T., and Wolski, K. (2015). "Mechanisms and kinetics of granulated sewage sludge combustion," *Waste Manage.* 46, 459-471. DOI: 10.1016/j.wasman.2015.08.015

Kijo-Kleczkowska, A., Środa, K., Kosowska-Golachowska, M., Musiał, T., and Wolski, K. (2016). "Combustion of pelleted sewage sludge with reference to coal and biomass," *Fuel* 170, 141-160. DOI: 10.1016/j.fuel.2015.12.026

Kijo-Kleczkowska, A., Środa, K., Kosowska-Golachowska, M., Musiał, T., and Wolski, K. (2016). "Experimental research of sewage sludge with coal and biomass co-combustion, in pellet form," *Waste Manage.* 53, 165-181. DOI: 10.1016/j.wasman.2016.04.021

Kulikowska, D. (2016). "Kinetics of organic matter removal and humification progress during sewage sludge composting," *Waste Manage.* 49, 196-203. DOI: 10.1016/j.wasman.2016.01.005

Kumar, R., and Singh, R. I. (2017). "An investigation of co-combustion municipal sewage sludge with biomass in a 20 kW BFB combustor under air-fired and oxygen-enriched condition," *Waste Manage.* 70, 114-126. DOI: 10.1016/j.wasman.2017.09.005

Li, J., Paul, M. C., Younger, P. L., Watson, I., Hossain, M., and Welch, S. (2016). "Prediction of high-temperature rapid combustion behaviour of woody biomass particles," *Fuel* 165, 205-214. DOI: 10.1016/j.fuel.2015.10.061

Li, Q., Jiang, J., Zhang, Q., Zhou, W., Cai, S., Duan, L., Ge, S., and Hao, J. (2016). "Influences of coal size, volatile matter content, and additive on primary particulate matter emissions from household stove combustion," *Fuel* 182, 780-787. DOI: 10.1016/j.fuel.2016.06.059

Liao, Y., Wu, S., Chen, T., Cao, Y., and Ma, X. (2015). "The alkali metal characteristic during biomass combustion with additives," *Energy Procedia* 75, 124-129. DOI: 10.1016/j.egypro.2015.07.209

Lin, Y., Liao, Y., Yu, Z., Fang, S., and Ma, X. (2017). "The investigation of co-

combustion of sewage sludge and oil shale using thermogravimetric analysis," *Thermochim. Acta* 653, 71-78. DOI: 10.1016/j.tca.2017.04.003

Link, S., Yrjas, P., and Hupa, L. (2018). "Ash melting behaviour of wheat straw blends with wood and reed," *Renew. Energ.* 124, 11-20. DOI: 10.1016/j.renene.2017.09.050

Liu, N. A., Fan, W., Dobashi, R., and Huang, L. (2002). "Kinetic modeling of thermal decomposition of natural cellulosic materials in air atmosphere," *J. Anal. Appl. Pyrol.* 63(2), 303-325. DOI: 10.1016/S0165-2370(01)00161-9

López, R., Fernández, C., Cara, J., Martínez, O., and Sánchez, M. E. (2014). "Differences between combustion and oxy-combustion of corn and corn – rape blend using thermogravimetric analysis," *Fuel Process. Technol.* 128, 376-387. DOI: 10.1016/j.fuproc.2014.07.036

Munir, S., Daood, S. S., Nimmo, W., Cunliffe, A. M., and Gibbs, B. M. (2009). "Thermal analysis and devolatilization kinetics of cotton stalk, sugar cane bagasse and shea meal under nitrogen and air atmospheres," *Bioresource Technol.* 100(3), 1413-1418. DOI: 10.1016/j.biortech.2008.07.065

Papari, S., and Hawboldt, K. (2015). "A review on the pyrolysis of woody biomass to bio-oil: Focus on kinetic models," *Renew. Sust. Energ. Rev.* 52, 1580-1595. DOI: 10.1016/j.rser.2015.07.191

Peng, X., Ma, X., and Xu, Z. (2015). "Thermogravimetric analysis of co-combustion between microalgae and textile dyeing sludge," *Bioresource Technol.* 180, 288-295. DOI: 10.1016/j.biortech.2015.01.023

Qi, J., Han, K., Wang, Q., and Gao, J. (2017). "Carbonization of biomass: Effect of additives on alkali metals residue, SO_2 and NO emission of chars during combustion," *Energy* 130, 560-569. DOI: 10.1016/j.energy.2017.04.109

Roy, P., Dutta, A., Acharya, B., and Deen, B. (2018). "An investigation of raw and torrefied lignocellulosic biomasses with CaO during combustion," *J. Energy Inst.* 91(4), 584-594. DOI: 10.1016/j.joei.2017.03.002

Shang, H., Lu, R.-R., Shang, L., and Zhang, W.-H. (2015). "Effect of additives on the microwave-assisted pyrolysis of sawdust," *Fuel Process. Technol.* 131, 167-174. DOI: 10.1016/j.fuproc.2014.11.025

Shen, D. K., Gu, S., Luo, K. H., Bridgwater, A. V., and Fang, M. X. (2009). "Kinetic study on thermal decomposition of woods in oxidative environment," *Fuel* 88(6), 1024-1030. DOI: 10.1016/j.fuel.2008.10.034

Singh, K., and Zondlo, J. (2017). "Characterization of fuel properties for coal and torrefied biomass mixtures," *J. Energy Inst.* 90(4), 505-512. DOI: 10.1016/j.joei.2016.05.012

Syed-Hassan, S. S. A., Wang, Y., Hu, S., Su, S., and Xiang, J. (2017). "Thermochemical processing of sewage sludge to energy and fuel: Fundamentals, challenges and considerations," *Renew. Sust. Energ. Rev.* 80, 888-913. DOI: 10.1016/j.rser.2017.05.262

Szemmelveisz, K., Szűcs, I., Palotás, Á. B., Winkler, L., and Eddings, E. G. (2009). "Examination of the combustion conditions of herbaceous biomass," *Fuel Process. Technol.* 90(6), 839-847. DOI: 10.1016/j.fuproc.2009.03.001

Tang, Y., Ma, X., and Lai, Z. (2011). "Thermogravimetric analysis of the combustion of microalgae and microalgae blended with waste in N_2/O_2 and CO_2/O_2 atmospheres," *Bioresource Technol.* 102(2), 1879-1885. DOI: 10.1016/j.biortech.2010.07.088

Wang, L., Skreiberg, Ø., and Becidan, M. (2014). "Investigation of additives for preventing ash fouling and sintering during barley straw combustion," *Appl. Therm.*

Eng. 70(2), 1262-1269. DOI: 10.1016/j.applthermaleng.2014.05.075

Wang, M., Chen, Z., Lv, J., Ren, Y., Jiang, Y., Jiang, E., and Wang, D. (2018). "Combustion characteristics and kinetic analysis of heavy tar from continuous pyrolysis of camellia shell," *Fuel Process. Technol.* 176, 131-137. DOI: 10.1016/j.fuproc.2018.03.015

Wang, S., Jiang, X. M., Han, X. X., Liu, J. G. (2009). "Combustion characteristics of seaweed biomass. 1. Combustion characteristics of *Enteromorpha clathrata* and *Sargassum natans*," *Energ. Fuel* 23(10), 5173-5178. DOI: 10.1021/ef900414x

Wang, X., Deng, S., Tan, H., Adeosun, A., Vujanović, M., Yang, F., and Duić, N. (2016). "Synergetic effect of sewage sludge and biomass co-pyrolysis: A combined study in thermogravimetric analyzer and a fixed bed reactor," *Energ. Convers. Manage.* 118, 399-405. DOI: 10.1016/j.enconman.2016.04.014

White, J. E., James Catallo, W., and Legendre, B. L. (2011). "Biomass pyrolysis kinetics: A comparative critical review with relevant agricultural residue case studies," *J. Anal. Appl. Pyrol.* 91(1), 1-33. DOI: 10.1016/j.jaap.2011.01.004

Xie, Z., and Ma, X. (2013). "The thermal behaviour of the co-combustion between paper sludge and rice straw," *Bioresource Technol.* 146, 611-618. DOI: 10.1016/j.biortech.2013.07.127

Yang, Y. B., Sharifi, V. N., and Swithenbank, J. (2004). "Effect of air flow rate and fuel moisture on the burning behaviours of biomass and simulated municipal solid wastes in packed beds," *Fuel* 83(11-12), 1553-1562. DOI: 10.1016/j.fuel.2004.01.016

Zhang, Q., Liu, H., Zhang, X., Xing, H., Hu, H., and Yao, H. (2017). "Novel utilization of conditioner CaO for gas pollutants control during co-combustion of sludge and coal," *Fuel* 206, 541-545. DOI: 10.1016/j.fuel.2017.06.044

Zhou, L., Wang, Y., Huang, Q., and Cai, J. (2006). "Thermogravimetric characteristics and kinetic of plastic and biomass blends co-pyrolysis," *Fuel Process. Technol.* 87(11), 963-969. DOI: 10.1016/j.fuproc.2006.07.002

Article submitted: July 27, 2018; Peer review completed: October 28, 2018; Revised version received: November 27, 2018; Accepted: December 19, 2018; Published: January 8, 2019.
DOI: 10.15376/biores.14.1.1466-1481